Electronic structure and correlation in β−Ti3O5 and λ−Ti3O5 studied by hard x-ray photoelectron spectroscopy

doi: 10.1103/PhysRevB.95.085133

Electronic structure and correlation in β-Ti_3O_5 and λ-Ti_3O_5 studied by hard x-ray photoelectron spectroscopy

Keisuke Kobayashi,[1,2,3] Munetaka Taguchi,[4] Masaaki Kobata,[5] Kenji Tanaka,[6] Hiroko Tokoro,[7] Hiroshi Daimon,[4] Tetsuo Okane,[1] Hiroshi Yamagami,[1] Eiji Ikenaga,[8] and Shin-ichi Ohkoshi[6,*]

[1]*Materials Sciences Research Center, Japan Atomic Energy Agency, 1-1-1 Kouto, Sayo-cho, Hyogo, 679-5148, Japan*

[2]*Research Institute of KUT, Kouchi University of Technology, Tosayamada, Kami City, Kochi 782-8502, Japan*

[3]*Hiroshima Synchrotron Radiation Center HiSOR, Hiroshima University, 2-313 Kagamiyama, Higashi-Hiroshima City, 739-0046 Japan*

[4]*Graduate School of Materials Science, Nara Institute of Science and Technology (NAIST), Ikoma, Nara 630-0192, Japan*

[5]*Collaborative Laboratories for Advanced Decommissioning Science, Japan Atomic Energy Agency, 2-4 Shirakata, Tokai-mura, Naka-gun, Ibaraki 319-1195, Japan*

[6]*Department of Chemistry, School of Science, University of Tokyo, 7-3-1 Hongo, Bunkyo-ku, Tokyo 113-0033, Japan*

[7]*Division of Materials Science, Faculty of Pure and Applied Sciences, University of Tsukuba, 1-1-1 Tennodai, Tsukuba, Ibaraki 305-8573, Japan*

[8]*SPring-8/JASRI, 1-1-1 Kouto, Sayo-cho, Hyogo, 679-5148, Japan*

(Received 17 February 2016; revised manuscript received 25 January 2017; published 22 February 2017)

We have conducted hard x-ray photoelectron spectroscopy investigations of the electronic structure changes and electron correlation phenomena which take place upon the photoinduced reversible phase transition between β- and λ-Ti_3O. From valence band spectra of β- and λ-Ti_3O_5, we have identified the bipolaron caused by the σ-type bonding of d_{xy} orbitals in β-Ti_3O_5 and the π stacking between the d_{xy} orbitals between different Ti sites in λ-Ti_3O_5, previously predicted by *ab initio* calculations. This indicates that the single electron band picture is valid for the description of photoinduced phase transitions. On the other hand, the Ti $2p$ and Ti $1s$ core level spectra exhibit nonlocal screening satellite features, which are typical spectroscopic signs of strong electron correlation in the coherent Ti t_{2g} states. The most striking result we obtain is that correlation in the valence band also manifests to reduce the plasmon energy, which results in an enhancement of the valence electron mass by a factor of 2.7.

DOI: 10.1103/PhysRevB.95.085133

I. INTRODUCTION

The titanium oxides family, which includes the very common TiO_2 used as an optical coating and a white pigment, is now attracting wide interest for use as advanced functional materials for practical applications in resistance memories, solar cells, photocatalysts, gas sensors, and so on. The titanium oxides exhibit a range of physical and chemical properties. From a basic scientific viewpoint, Ti_nO_{2n-1} in particular are very interesting materials, which occupy a position at the boundary between weak and strong electron correlation and exhibit crystalline polymorphism. The on-site Coulomb interaction in Mott-Hubbard systems such as the titanium oxides is expected to be smaller ($\sim$5.5 eV) than the 8 eV for typical strong correlation materials [1]. Taguchi *et al.* have reported the manifestation of strong correlation effects in hard x-ray photoelectron spectroscopy (HXPES, or HAXPES) spectral investigations of the sequential structural phase transition in Ti_4O_7 [2]. The $3d$ electron states, which are localized near the Fermi level, were found to be relevant to the varieties of polymorphism, which are related to rich functional properties.

Ohkoshi and co-workers [3,4] synthesized a flake form sample of unique λ-Ti_3O_5 phase nanocrystalline flakes, and reported a photoreversible phase transition at room temperature between the λ-Ti_3O_5 and β-Ti_3O_5 phases. A repeated sequence of irradiation at 532 and 410 nm was found to induce a reversible black-brown cyclic color change. Furthermore, Tokoro *et al.* [5,6] have very recently discovered an externally controllable heat storage effect under the pressure-and-heat, pressure-and-light, and pressure-and-current reversible phase transitions. These findings have led to a major resurgence of interest in titanium oxides and shown the importance of new oxide heat storage, sensor, and switching memory device based on Ti_3O_5. Based on XRD and optical absorption measurements, *ab initio* calculations, and thermodynamic analysis, they concluded that this phenomenon can be understood as a photoinduced metal-semiconductor transition due to a change in crystal structure from the metastable λ-Ti_3O_5 phase, to the truly stable β-Ti_3O_5 phase [3,4]. A brief explanation of these exotic phenomena with schematic illustrations is given in the Supplemental Material [7]. If Ohkoshi *et al.*'s interpretation is correct, electron correlation does not play a role in the phase change phenomena, in contrast to the Ti_4O_7 case. Is electron correlation negligibly small in Ti_3O_5? Experimental investigations of electronic structure are necessary to clarify this point.

In this article we report an investigation of the electronic structure of λ-Ti_3O_5 and β-Ti_3O_5 using HXPES, which offers much higher bulk sensitivities than conventional PES, and avoids the surface effects of the nanocrystalline flake samples [8–10]. While the valence band spectra revealed that the valence band spectra of β- and λ-Ti_3O_5 coincide well with simulated spectra from DFT density of states calculations, the core-level spectra reveal strong electron correlation of Ti $3d$. The most interesting finding of the present study is the observation of a series of satellites with equal energy spacing in all of the observed O and Ti spectra, which cannot be attributed to charge transfer excitations. We identify these as loss features due to valence plasmon excitations, with reduced energy due to valence electron mass enhancement by a factor of 2.7. We

*Correponding author: ohkoshi@chem.s.u-tokyo.ac.jp

also discuss the origins of weaker satellites observed in the core level spectra.

II. EXPERIMENT

Nanoflake Ti_3O_5 samples were prepared by the Ohkoshi group at the University of Tokyo. Details of the preparation are explained in Ref. [3]. We performed HXPES measurements of valence band and core levels at a x-ray photon energy of 8 keV with total energy resolution of 0.3 eV at BL47XU of SPring-8. All the measurements were done at room temperature. The valence band spectra are compared with the first principle DFT calculations of Ohkoshi *et al.* [3,4] using the Vienna *ab initio* simulation package (VASP) to discuss the electronic structure change due to the phase transition. Parameters for the on-site Coulomb interaction U and the exchange interaction J are used to include correlation effects with $U - J = 5.0$ eV in these calculations [3]. We also discuss the core level spectra based on a cluster calculation by Taguchi [11–14] in order to estimate the effects of electron correlation.

III. RESULTS AND DISCUSSIONS

A. Valence band spectra and DFT calculation

Figure 1(a) shows a superposition of experimental valence band spectra, following Shirley background subtraction, and normalized by the integrated intensities, for β-Ti_3O_5 phase and λ-Ti_3O_5 phase samples. The spectra are similar, except a distinct increase of the spectral weight for the β-Ti_3O_5 spectrum in the binding energy region between 6.5 and 8.5 eV. A weaker structure appears beneath the Fermi level in both spectra, as shown in Fig. 1(b) in enlarged scale with dots. Curve fittings were done for the two spectra using Voigt functions with Shirely backgrounds to discuss the difference. The results are shown with solid curves for fitted spectra and dotted curves for the Voigt functions and background. The λ-phase spectrum exhibits a single peak at 0.66 eV with a long tail down toward the main band. The onset coincides with the Fermi level, indicating no gap due to empty states. For the β phase, the structure consists of two components with peaks at binding energy of 1.2 and 0.56 eV. An energy gap of 0.2 eV can be distinguished between the onset and the Fermi level.

Figures 2(a) and 2(b), show calculated total and partial densities of states (TDOS and PDOS, respectively) of the valence band for the β and λ phases. The broad bands between 3.5 and 8.5 eV mainly consist of O $2p$ orbitals. States originating in Ti p and d, which are hybridized with O $2p$, are distributed smoothly over this region. Ti s states peak at a binding energy of around 8 eV with narrower widths, suggesting a certain degree of localized nature. The band gaps between the O $2p$ band and the conduction band in the calculation are 3.6 and 4.1 eV for the β and λ phase, respectively. The localized t_{2g} states, which appear in the band gap region, show a double-peaks feature for the β-phase sample. A small gap of 100 meV is recognizable beneath the conduction band onsets. There are three different Ti sites in a unit cell of Ti_3O_5, as denoted by Ti(1), Ti(2), and Ti(3) depicted in Fig. 3. The deeper peak, at 1.5 eV in Fig. 2(b) for the β phase, is due to the Ti(1)-Ti(1) dimer. The lower binding energy peak at around 0.6 eV can be assigned to a

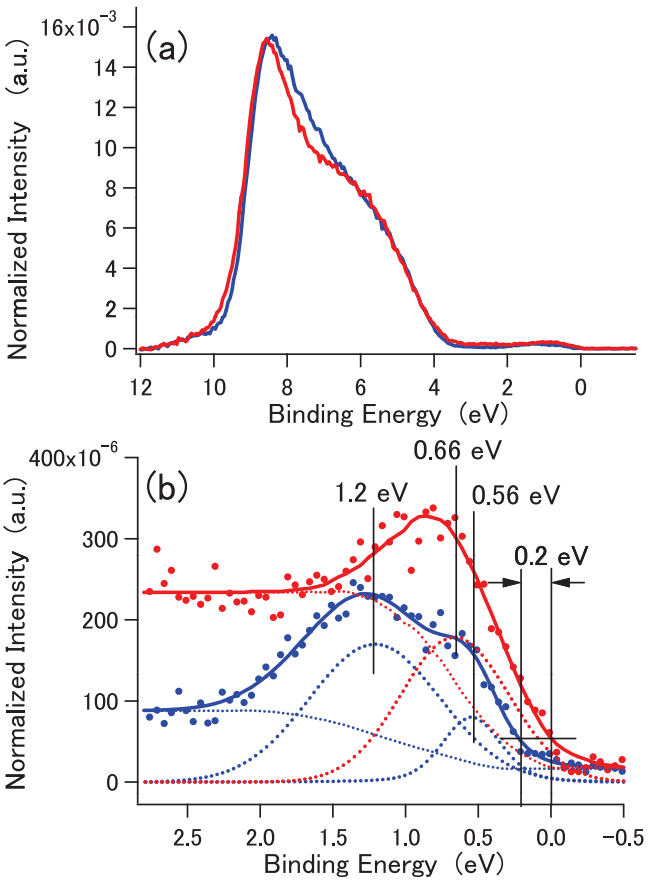

FIG. 1. (a) Comparison of experimental valence band spectra for the β (blue) and λ (red) phases, respectively. These spectra have been normalized to integrated intensity after eliminations of Shirley backgrounds. (b) Blue and red dots show the data points of experimental spectra in the band gap region beneath the Fermi level for the β and λ phases, respectively, on an enlarged scale. The blue and red curves are curve-fit results for the two phases, and the dashed curves show the individual Voigt function components and backgrounds. It is clear that the t_{2g} state in the λ phase (red) is well fitted by a single Voigt function with an intense background in the band gap region between the t_{2g} states and O $2p$-like main band. For the β phase (blue), two Voigt components with a weaker background are necessary to fit the experimental spectra. The onset of the λ-phase spectrum just coincides with the Fermi level, whereas onset of the β-phase spectrum is 0.2 eV below the Fermi level.

bipolaron due to σ bonding of Ti(3)-Ti(3) d_{xy} orbitals [3]. The peaks at +0.71 eV above the Fermi level can be assigned to the d_{xz} orbital on Ti(2). In the λ phase, the t_{2g} state of the Ti(1)-Ti(1) dimer peaks at 0.58 eV, as shown in Fig. 2(a). Slipped π stacking of d_{xy} orbitals on Ti(2) and Ti(3) forms states which extend to the conduction band, over the Fermi level [3,4], bringing the metallic nature to the λ phase.

The thick solid curves in Figs. 2(c) and 2(d) are least mean square fitting results of linear combinations of PDOSs (thin solid curves) to the experimental spectra. It is apparent that the photoionization cross sections strongly modify the spectral shape [15,16]. The Ti s and Ti p PDOSs contribute considerably to the spectral weight in the main O p-like valence band, whereas Ti d gives a weaker contribution. There is an apparent difference between the simulated and

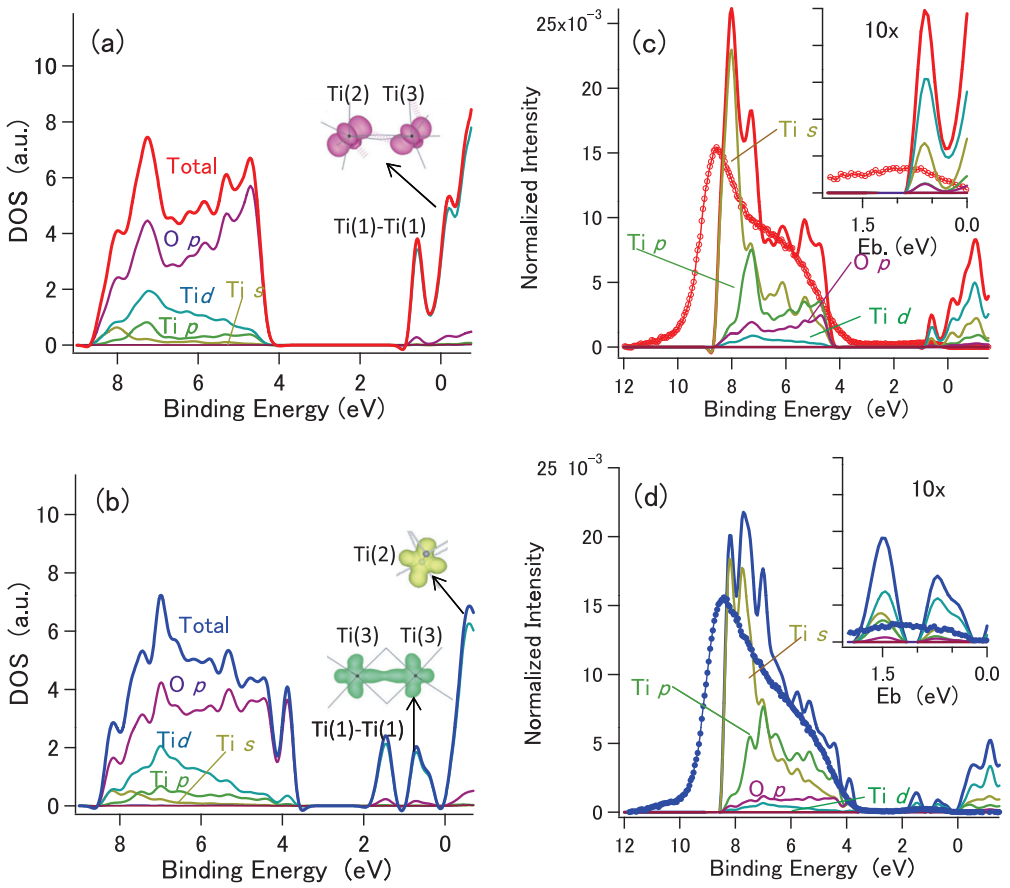

FIG. 2. (a) and (b) DOSs and PDOSs. (c) and (d) Comparisons of experimental and simulated spectra for the λ phase [(a) and (c)] and β phase [(b) and (d)], respectively. The experimental and simulated t_{2g} spectra are shown on enlarged scales in the inset to (c) and (d).

experimental spectra near the bottom of the valence band. The simulated spectra show sharp peaks at 8.0 eV due to intense Ti s contributions, whereas the experimental spectra for both the β and λ phases peak at 8.5 eV, with broader widths. Consequently, the experimental valence bandwidths are more than 1 eV wider than those of simulated spectra. This difference is due to the corelike nature of the Ti 4s state. A hole generated in a core level with narrow width can interact with the outgoing photoelectron, giving rise to a decrease in kinetic energy (or an increase in binding energy). This effect is proportional to the width of the relevant ground state. Shifts of around 1 eV compared to the DFT-calculated peak positions have been observed for shallow corelike states with 0.5–1 eV calculated widths in various compounds [9]. The valence band spectral shape difference in the 6.5–8.5 eV region, shown in Fig. 1, can be attributed to the differences in the Ti p and O p PDOSs between the β and λ phases. The O p PDOS in this region in the λ phase shows apparent dip, whereas that in the β phase is rather flat. The Ti p PDOS, which gives the second largest contribution to the valence band spectrum, exhibits a similar behavior. Consequently, the valence band spectral weight is smaller for the λ phase than the β phase in this energy region.

Regarding the t_{2g} states, curve-fitting analyses of the experimental spectra reveal two peaks at 1.2 and 0.56 eV in the β phase, and a single peak at 0.66 eV in the λ phase as shown in Fig. 1(b). These can be reasonably attributed to the Ti(1)-Ti(1) dimer, and the bipolaron due to the σ bonding of the Ti(3)-Ti(3) d_{xy} orbitals for the β phase, and the Ti(1)-Ti(1) dimer for the λ phase. The intensities of these t_{2g} features are weaker and the widths are broader than the simulated spectra as shown in the subfigures of Figs. 2(c) and 2(d). These discrepancies are presumably due to randomness caused by imperfect crystallinity in the flake form samples. Spectral weight is transferred to the energy gap region between the O 2p-like main band and the t_{2g} states, forming distinctive long tails towards onsets of the O 2p-like main bands as seen in Fig. 1(b).

In our discussion we have neglected photoelectron recoil effects [17], which may be observable in materials consisting of light elements such as O and Ti. The sizes of effects can be estimated from $(m/M)E_k$, where m, M, and E_k are the electron mass, the atomic mass, and the kinetic energy of the photoelectron, respectively. For the O 1s and Ti 2p core spectra these estimates are as 0.25 and 0.086 eV, respectively, suggesting that the recoil effects are comparable to the total resolution of the present experiments for O, and negligibly smaller for Ti. We thus consider that modifications of the recoil effects due to chemical bonding differences between the two crystallographic phases are not likely to be large enough to affect our discussions on the spectral differences between the two phases.

The simulated spectra based upon *ab initio* calculations with U explain well the observed valence band spectra, providing a sound basis for understanding the λ- and β-phase change in Ti_3O_5 as a semiconductor-metal transition in a single electron band structure picture. Since the energies of

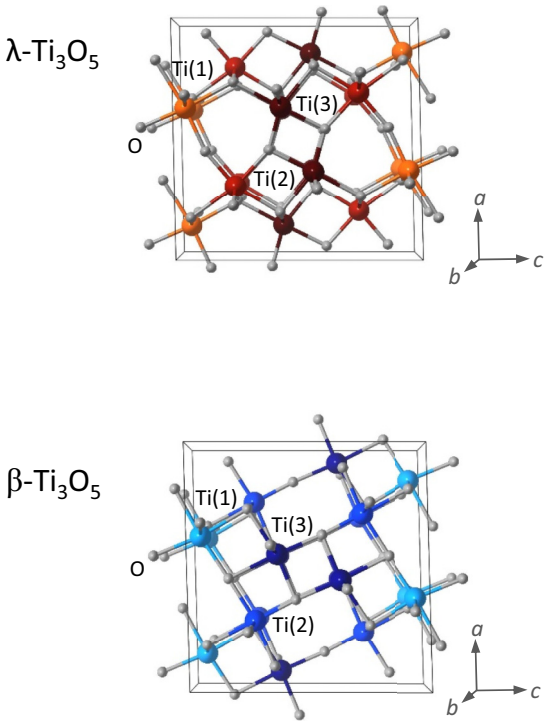

FIG. 3. Unit cells of β phase [(a) and (c)] and λ phase Ti_3O_5. The three different sites of Ti atoms are indicated as Ti(1), Ti(2), and Ti(3).

the photoexcitations necessary to cause the structural change are smaller than the energy gap between the main filled O $2p$ band and the empty band, which is around 4 eV, the phase transition can be considered as being due to electron excitation from the filled t_{2g} states to higher empty bands.

B. Nonlocal screening features in the Ti $2p$ core spectra

The curves shown in Fig. 4(a) are the Ti $2p$ spectra of the β and λ phase. The peaks at 459.36 and 465.0 eV can be assigned to the $2p_{3/2}$–$2p_{1/2}$ spin-orbit doublet for each spectrum. In the β phase, a prominent satellite of the $2p_{3/2}$ peak is clearly seen at 457.51 eV (denoted by A), whereas a broad shoulder can be recognized at around 457.81 eV in the λ phase. A similar behavior of the satellites (denoted by A′) can also be recognized in the spin-orbit counterpart in the β-phase spectrum. In order to make the difference in structure A between the two phases clearer, the main peak and satellite were separated using Voigt functions after subtraction of Shirley backgrounds. The results are shown in Fig. 4(c). Unexpectedly, the relative spectral weights of the satellites are not much different (0.29 and 0.25) between the β and λ phases. The apparent difference is due to broadening and a peak shift toward higher binding energy of the satellite in the λ phase. These low binding energy satellites have been identified as the well-screened final state of $\underline{2p}\ 3d^1\underline{C}$, where C and the underbar denote the coherent t_{2g} state near E_F and a hole in the state, respectively [11–14]. We fit the experimental spectra for both the β and λ phase by changing the charge transfer energy Δ, Δ^*, and V^* in the cluster calculations. The best fit was obtained for $\Delta = 4.9$ eV, $\Delta^* = 0.0$ eV, and $V^*(e_g) = 0.384$ eV for the λ phase, $\Delta = 5.3$ eV, $\Delta^* = 0.2$ eV,

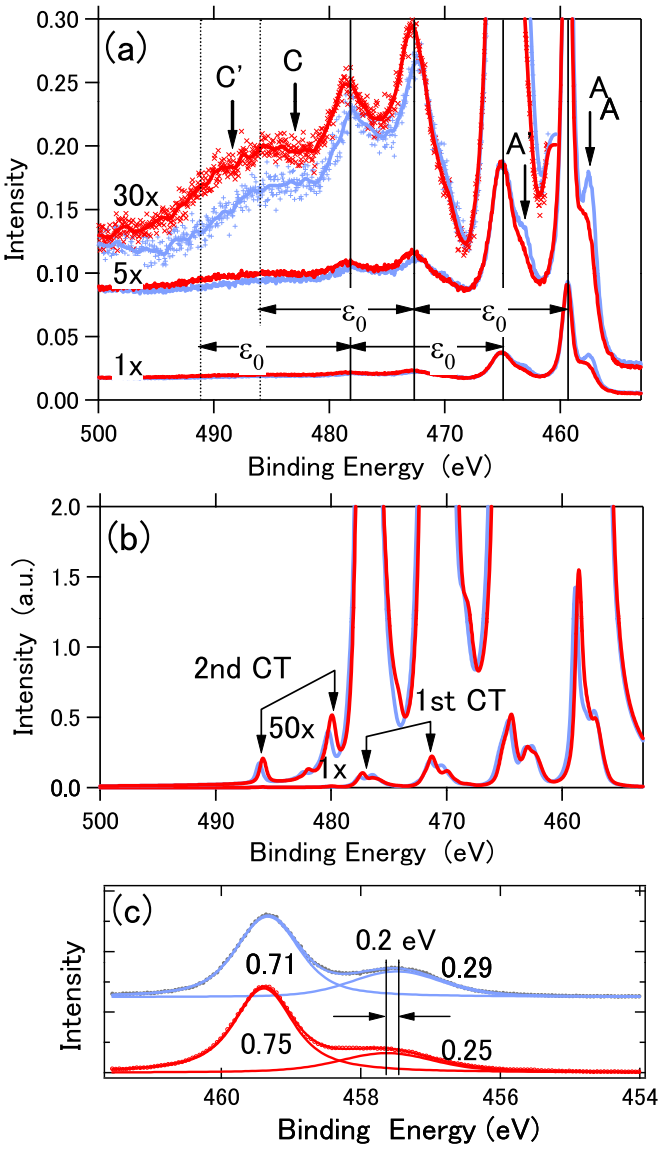

FIG. 4. Experimental (a) and simulated (b) Ti $2p$ spectra, shown at different vertical magnifications. In the highest magnification (30×) experimental spectra, the data points are shown by dots, and 30 point smoothed spectra are shown by solid curves. The gray and black (thin blue and red) represent the β and λ phases, respectively. (c) The main and lower energy satellite peaks (A) of Ti$2p_{3/2}$ are separated by fitting using two Voigt functions after subtracting Shirley backgrounds for the β (gray, thin blue on line) and λ (black, red on line) phases.

and $V^*(e_g) = 0.448$ eV for the β phase. All the other parameter values were fixed: $U_{dd} = 7.0$ (on-site repulsive Coulomb interaction between the Ti $3d$ states), $U_{dc} = 8.8$ (the attractive $2p$ core-hole potential), $10\mathrm{Dq} = 0.2, D_{\mathrm{trg}} = 0.05$ (a small trigonal crystal field), and $V(e_g) = 3.2$, in units of eV. An effective coupling parameter for describing the interaction strength between the central Ti $3d$ orbital and the coherent band V^* was introduced analogous to the hybridization V. The Δ^* parameter is defined as the energy difference of the configuration-averaged energies $E(3d^1C)$-$E(3d^0)$. The cluster calculation reproduces the well-screened satellite components in both phases as shown by the curves in Fig. 4(b). This

simulation gives the occupations of the t_{2g} states as 0.639/atom and 0.657/atom for β and λ phases, respectively. These values are comparable with the values of 0.75/atom and 0.79/atom estimated by integration of the t_{2g} PDOS below E_F.

C. CT satellites vs plasmon satellites

Distinctive satellite features other than the nonlocal screening satellites appear in the Ti $2p$ experimental spectra at binding energies 13 eV higher than the main peaks. Similar satellites have been reported for various $3d$ transition metal oxides, including Ti oxides, and interpreted as charge transfer (CT) satellites [18,19]. Our cluster calculations well reproduce these 13 eV satellites due to CT excitations both for the λ and β phases as shown in Fig. 4(b). Weak peaks, which are identified as the second-order CT satellites of the $2p_{3/2}$-$2p_{1/2}$ spin-orbit doublet, appear in the higher binding energy region in the calculation, as shown in Fig. 4(b) on an enlarged vertical scale. The calculated energy separation between the second- and first-order CT satellites is 8.6 eV, about 4.4 eV smaller than observed 13 eV

Similar series of satellites are also distinct in the Ti $1s$ spectra as shown in Fig. 5(a). In both phases, up to three satellite structures appear at higher binding energies than the main Ti $1s$ peaks, with energy separations ε_0 of 13 eV, equal to those of Ti $2p$ satellites. Simulation of the Ti $1s$ spectra from the cluster calculations is shown in Fig. 5(b). The peak positions of the first satellite in the simulation and the experiment coincide well with the 13 eV separations from the main peaks. However, the simulation predicts the second CT satellite lies at a binding energy 8.6 eV higher than that of the first CT satellite, as in the case of the Ti $2p$ satellites. The strongest contribution to this reduction in the energy spacing comes from the relatively weaker hybridization between the ligand state and the double CT t_{2g} state compared to that between the ligand state and the single CT state. A smaller modification also comes from the repulsive interactions between multiply transferred charges from ligand O $2p$ states to empty t_{2g} states.

In order to further confirm the universality of the energy spacing, satellites in the O $2s$, Ti $3p$, Ti $3s$, O $1s$, and Ti $2s$ spectra were also investigated as shown in Figs. 6(a) and 6(b). All of the satellite peaks appear with the same energy spacing relative to the main peaks in these spectra. The average energy separation ε_0 of all of the observations are 13.1 ± 0.2 and 12.9 ± 0.1 eV for the β phase and λ phase, respectively. The CT excitation mechanism does not predict such equally spaced series of satellite structures as discussed above.

To our knowledge, plasmon energy losses are the only reasonable candidate for the 13 eV spaced satellites. Here the energy spacing is determined by the plasmon energy $\hbar\omega_p = \hbar\sqrt{\frac{4\pi ne^2}{m}}$, where n and m are the density and the mass of the valence electrons, respectively. For Si, the observed plasmon energy of 17.2 eV coincides with a calculation using a valence electron density of $0.199 \times 10^{24}/\mathrm{m}^3$ and the free electron mass. For Ti_3O_5, the numbers of density of valence electrons, which can contribute to the plasmon oscillation, can be estimated by subtracting the number of localized t_{2g} electrons from the apparent valence electron number of 32/molecule. The volumes of the unit cells, which contain four

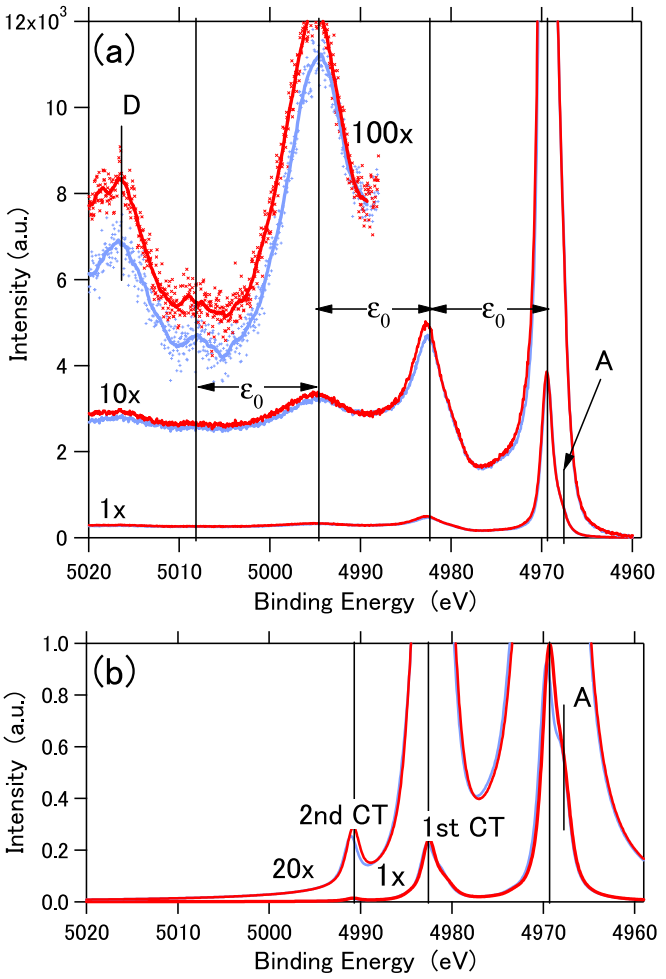

FIG. 5. Experimental (a) and simulated (b) Ti $1s$ spectra, shown at different vertical magnifications. In the highest magnification (100×) experimental spectra, the data points are shown by dots, and 30 point smoothed spectra are shown by solid curves. The gray and black (thin blue and red) represent the β and λ phases, respectively.

molecules, are $0.37135 \times 10^{-27}/\mathrm{m}^3$ and $0.37255 \times 10^{-27}/\mathrm{m}^3$ for β- and λ-Ti_3O_5, respectively. The corresponding valence band electron densities are thus $0.320 \times 10^{24}/\mathrm{m}^3$ and $0.318 \times 10^{24}/\mathrm{m}^3$, larger than that of Si. The only possible explanation of the experimental observation consistent with plasmon energy loss is to assume that the valence electron mass is enhanced in Ti_3O_5 with an effective mass $m^* = 2.7\,\mathrm{m}$ in both phases. In the tight-binding approximation, the effective mass of the band electrons is proportional to the inverse of the bandwidth. It is noteworthy to point out that a mass reduction factor of 2.7 is very near to the ratio of the calculated valence bandwidths of 2.4. (The DFT calculated valence bandwidth of Ti_3O_5 is 5 eV, whereas that of Si is 12 eV).

D. Other weak satellite features

Several additional features are seen in the experimental spectra. In Fig. 6(c) a broad weak structure B, with an onset around 4 eV above the O $1s$ main peak is distinguishable. This energy coincides with the band gap between the O $2p$ occupied band and E_F, indicating that B is the energy loss due to single valence electron excitation to the extended states. In

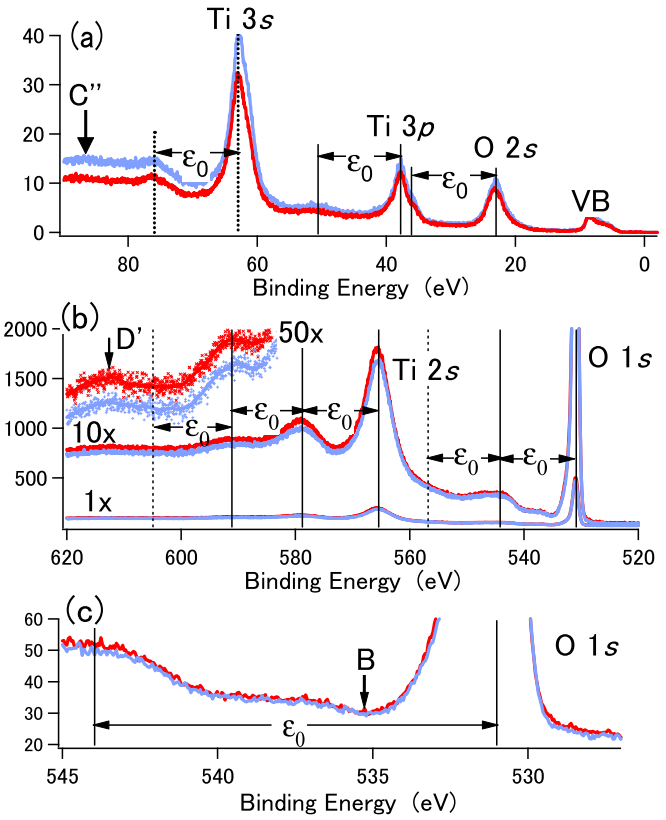

FIG. 6. (a) O 2*s*, Ti 3*p*, and Ti 3*s* spectra for the β (blue) and λ (red) phases. (b) O 1*s* and Ti 2*s* spectra for the β (gray, thin blue) and λ (black, red) phases. (c) O 1*s* spectra on an enlarged vertical scale.

Fig. 6(a), a weak feature C'' at 23.5 eV above the Ti 3*s* main peak is distinguishable. This energy difference coincides with the excitation energy (23.1 eV) of O 2*s* electrons to the Fermi level. Thus it is reasonable to assign C'' to an energy loss structure. The broad structures in the region of 480–495 eV in the Ti 2*p* spectra in Fig. 4 are likely to be superpositions of the second overtones of the 13 eV energy loss, and the energy loss peaks due to O 2*s* excitations of Ti2$p_{3/2}$ (C) and Ti2$p_{1/2}$ (C′) main peaks. The weak features D in Fig. 5 and D′ in Fig. 6(b) appear at binding energies 46.95 and 46.05 eV higher than the Ti 1*s* and Ti 2*s* main peaks, respectively. The most probable interpretation is that they are due to the intra-atomic excitation of a Ti 3*p* electron to empty states above the Fermi level. Since the binding energy of Ti 3*p* is 37.9 eV as seen in Fig. 5(a), we have to assume an intra-atomic hole-hole Coulomb interaction of 8–9 eV for this explanation. Indeed a Coulomb interaction of ∼8 eV is shown to be reasonable for the Ti 3*p* core hole interacting with the Ti 1*s* and Ti 2*s* core holes by the present cluster calculation.

IV. SUMMARY

Based upon the experimental results discussed above, we summarize the electronic nature of Ti_3O_5 as follows: the electronic structures of both β- and λ-Ti_3O_5 can be successfully explained by the single electron band picture, taking into account correlation by U. Consequently, the understanding of the photoinduced phase transition mechanism given by Ohkoshi *et al.* based on the combination of *ab initio* band calculations and a thermodynamic energy calculation using the Slichter and Drickamer mean-field model [20] is considered adequate. The same calculation exhibits the existence of localized coherent Ti 3*d* t_{2g} states beneath the Fermi level, already suggesting the importance of correlation. The core level spectra exhibit features due to correlation in these coherent states, consistent with single cluster calculations with an on-site Coulomb interaction of 7.0 eV and an interaction strength between the central Ti 3*d* orbitals and the coherent band V^* of around 0.4 eV. Both the t_{2g} states of Ti(2) and Ti(3) in λ-Ti_3O_5 are merged into the extended states, whereas the Ti(3) t_{2g} state remains localized in the β phase. A possible stronger hybridization of the extended t_{2g} states may be responsible for the weaker and broader well-screened satellite in the λ phase as compared to β-Ti_3O_5. Due to the narrow valence bandwidth of 5 eV, the effective mass of the valence band electrons is enhanced by a factor of 2.7 compared to the free electron mass. Three more satellite structures were observed in the present experiments. Two of these can be well interpreted as being energy losses due to single particle excitations from the valence band and O 2*s* to empty states. The remaining satellites are interpreted as intra-atomic excitations of Ti 3*s* to empty states, accompanied by Ti 1*s* and Ti 2*s* core-hole excitations with a hole-hole Coulomb interaction of 8–9 eV. Charge transfer satellites seem to be involved in the Ti 2*p* and Ti 1*s* spectra. However, this mechanism does not give a reasonable explanation of the observed satellites.

In conclusion, the present spectroscopic investigation shows that the photoinduced phase transition phenomena can be understood based on the single electron band picture as predicted by Ohkoshi *et al.* [3]. At the same time, it revealed that electron correlation effects manifest in an enhancement of valence electron mass by a factor of 2.7, as deduced from the reduction of the plasmon energy. Correlation effects are also distinct in the core level spectra. Although correlation effects seem not to affect the steady aspects in the phase transition, they may play roles in dynamical features such as transport phenomena and transient in short laser pulse induced phase transitions upon excitations in Ti_3O_5.

ACKNOWLEDGMENT

The present research was supported in part by a JSPS Grant-in-Aid for specially promoted Research (Grant No. 15H05697).

[1] M. Imada, A. Fujimori, and Y. Tokura, Rev. Mod. Phys. **70**, 1039 (1998).

[2] M. Taguchi, A. Chainani, M. Matsunami, R. Eguchi, Y. Takata, M. Yabashi, K. Tamasaku, Y. Nishino, T. Ishikawa, S. Tsuda,

S. Watanabe, C.-T. Chen, Y. Senba, H. Ohashi, K. Fujiwara, Y. Nakamura, H. Takagi, and S. Shin, Phys. Rev. Lett. **104**, 106401 (2010).

[3] S. Ohkoshi, Y. Tsunobuchi, T. Matsuda, K. Hashimoto, A. Namai, F. Hakoe, H. Tokoro, Nat. Chem. **2**, 539 (2010).

[4] See Ref. 3, supplementary information, http://www.nature.com/naturechemistry.

[5] H. Tokoro, M. Yoshikiyo, K. Imoto, A. Namai, T. Natsu, K. Nakagawa, N. Ozaki, F. Hakoe, K. Tanaka, K. Chiba, R. Makiura, K. Prassides, and S. Ohkashi, Nat. Commun. **6**, 7037 (2015).

[6] See Ref. 5, supplementary information, http://www.nature.com/naturecommunications.

[7] See Supplemental Material at http://link.aps.org/supplemental/10.1103/PhysRevB.95.085133 for details of exotic phenomena with schematic illustrations.

[8] K. Kobayashi, M. Yabashi, Y. Takata, T. Tokushima, S. Shin, K. Tamasaku, D. Miwa, T. shikawa, H. Nohira, T. Hattori, Y. Sugita, O. Nakatsuka, A. Sakai, and S. Zaima, Appl. Phys. Lett. **83**, 1005 (2003).

[9] K. Kobayashi, Nuclear Instrum. Methods Phys. Res. A **547**, 98 (2005).

[10] K. Kobayashi, Nuclear Instrum. Methods Phys. Res. A **601**, 32 (2009).

[11] K. Horiba, M. Taguchi, A. Chainani, Y. Takata, E. Ikenaga, D. Miwa, Y. Nishino, K. Tamasaku, M. Awaji, A. Takeuchi, M. Yabashi, H. Namatame, M. Taniguchi, H. Kumigashira, M. Oshima, M. Lippmaa, M. Kawasaki, H. Koinuma, K. Kobayashi, T. Ishikawa, and S. Shin, Phys. Rev. Lett. **93**, 236401 (2004).

[12] M. Taguchi, A. Chainani, N. Kamakura, K. Horiba, Y. Takata, M. Yabashi, K. Tamasaku, Y. Nishino, D. Miwa, T. Ishikawa, S. Shin, E. Ikenaga, T. Yokoya, K. Kobayashi, T. Mochiku, K. Hirata, and K. Motoya, Phys. Rev. B **71**, 155102 (2005).

[13] M. Taguchi, A. Chainani, K. Horiba, Y. Takata, M. Yabashi, K. Tamasaku, Y. Nishino, D. Miwa, T. Ishikawa, T. Takeuchi, K. Yamamoto, M. Matsunami, S. Shin, T. Yokoya, E. Ikenaga, K. Kobayashi, T. Mochiku, K. Hirata, J. Hori, K. Ishii, F. Nakamura, and T. Suzuki, Phys. Rev. Lett. **95**, 177002 (2005).

[14] M. Taguchi, M. Matsunami, Y. Ishida, R. Eguchi, A. Chainani, Y. Takata, M. Yabashi, K. Tamasaku, Y. Nishino, T. Ishikawa, Y. Senba, H. Ohashi, and S. Shin, Phys. Rev. Lett. **100**, 206401 (2008).

[15] J. J. Yeh and I. Lindau, At. Data Nucl. Data Tables **32**, 1 (1985).

[16] M. B. Trzhaskovskaya, V. K. Nikulin, V. I. Nefedov, and V. G. Yarzhemsky, At. Data Nucl. Data Tables **92**, 245 (2006).

[17] Y. Takata, Y. Kayanuma, M. Yabashi, K. Tamasaku, Y. Nishino, D. Miwa, Y. Harada, K. Horiba, S. Shin, S. Tanaka, E. Ikenaga, K. Kobayashi, Y. Senba, H. Ohashi, and T. Ishikawa, Phys. Rev. B **75**, 233404 (2007).

[18] K. S. Kim and N. Wimograd, Chem. Phys. Let. **31**, 312 (1975).

[19] A. E. Bocquet, T. Mizokawa, K. Morikawa, A. Fujimori, S. R. Barman, K. Maiti, D. D. Sarma, Y. Tokura, and M. Onoda, Phys. Rev. B **53**, 1161 (1996).

[20] C. P. Slichter and H. G. Drickamer, J. Chem. Phys. **56**, 2142 (1972).